RMetS

Royal Meteorological Society

Greenland Blocking Index 1851–2015: a regional climate change signal

Edward Hanna,[a]* Thomas E. Cropper,[b] Richard J. Hall[a] and John Cappelen[c]

[a] *Department of Geography, University of Sheffield, UK*
[b] *Scientific Figure Design, Sheffield, UK*
[c] *Danish Meteorological Institute, Copenhagen, Denmark*

ABSTRACT: We present an extended monthly and seasonal Greenland Blocking Index (GBI) from January 1851 to December 2015, which more than doubles the length of the existing published GBI series. We achieve this by homogenizing the Twentieth Century Reanalysis version 2c-based GBI and splicing it with the NCEP/NCAR Reanalysis-based GBI. For the whole time period, there are significant decreases in GBI in autumn, October and November, and no significant monthly, seasonal or annual increases. More recently, since 1981 there are significant GBI increases in all seasons and annually, with the strongest monthly increases in July and August. A recent clustering of high GBI values is evident in summer, when 7 of the top 11 values in the last 165 years – including the two latest years 2014 and 2015 – occurred since 2007. Also, 2010 is the highest GBI year in the annual, spring, winter and December series but 2011 is the record low GBI value in the spring and April series. Moreover, since 1851 there have been significant increases in GBI variability in May and especially December. December has also shown a significant clustering of extreme high and low GBI values since 2001, mirroring a similar, recently identified phenomenon in the December North Atlantic Oscillation index, suggesting a related driving mechanism. We discuss changes in hemispheric circulation that are associated with high compared with low GBI conditions. Our GBI time series should be useful for climatologists and other scientists interested in aspects and impacts of Arctic variability and change.

KEY WORDS   blocking; climate change; GBI; Greenland; NAO; pressure

1. Introduction

High-pressure blocking over Greenland has been of great interest to weather forecasters and climatologists for many years. This blocking has traditionally been discussed in quite descriptive terms but more recently a Greenland Blocking Index (GBI) has been defined by Fang (2004) and popularized by Hanna *et al.* (2013, 2014, 2015), where GBI is the mean 500 hPa geopotential height for the 60–80°N, 20–80°W region (Figure 1). A basic GBI dataset has recently been made available on the US National Oceanographic and Atmospheric Administration (NOAA)'s Earth System Research Laboratory Physical Sciences Division at: http://www.esrl.noaa.gov/psd/data/timeseries/daily/GBI/ but, in common with the above-referenced work, it only extends back to 1948. The GBI represents, and clearly depicts changes in, blocking across the entire Greenland region. A comparison with the blocking index of Davini *et al.* (2012), which is based on a considerably smaller subset of the GBI region (62.5–72.5°N, 20–70°W), shows very strong agreement with the GBI: the two series are correlated at ≥0.98 based on monthly data from

NCEP/NCAR Reanalysis for 1948 to near present. Similarly, the Absolute Geopotential Height blocking measure of Scherrer *et al.* (2006) shows a preferential blocking region centred over Greenland, which is effectively captured through the GBI. Instantaneous anticyclonic blocking over both Greenland and Siberia has also been observed by Davini *et al.* (2012, 2013), who related it to Northern Hemisphere jet-stream flow. Overland *et al.* (2015) discuss changes in both of these regional blocking features, which appear to be related to a more amplified northern polar jet stream during the last 10–20 years of Arctic Amplification (Francis and Vavrus, 2015).

Here we extend the GBI back to 1851 using the newly available Twentieth Century Reanalysis version 2c (20CRv2c; Compo *et al.*, 2011, 2015) and are thus able to place previously published studies on observed GBI changes in the last 67 years in a much longer-term (165-year) climatic context. A great advantage of 20CRv2c data is the provision of data back to the mid-19th century, purely reliant on surface measurements, which avoids homogeneity issues in the satellite records caused for example by changes in satellite technology. However, recent work (Ferguson and Villarini, 2012, 2014; Wang *et al.*, 2013) has highlighted homogeneity issues in the 20CR data, some of which are likely to be non-climatic in origin, that we attempt to remove through homogeneity testing.

* Correspondence to: E. Hanna, Department of Geography, University of Sheffield, Winter Street, Sheffield, S10 2TN UK. E-mail: ehanna@sheffield.ac.uk
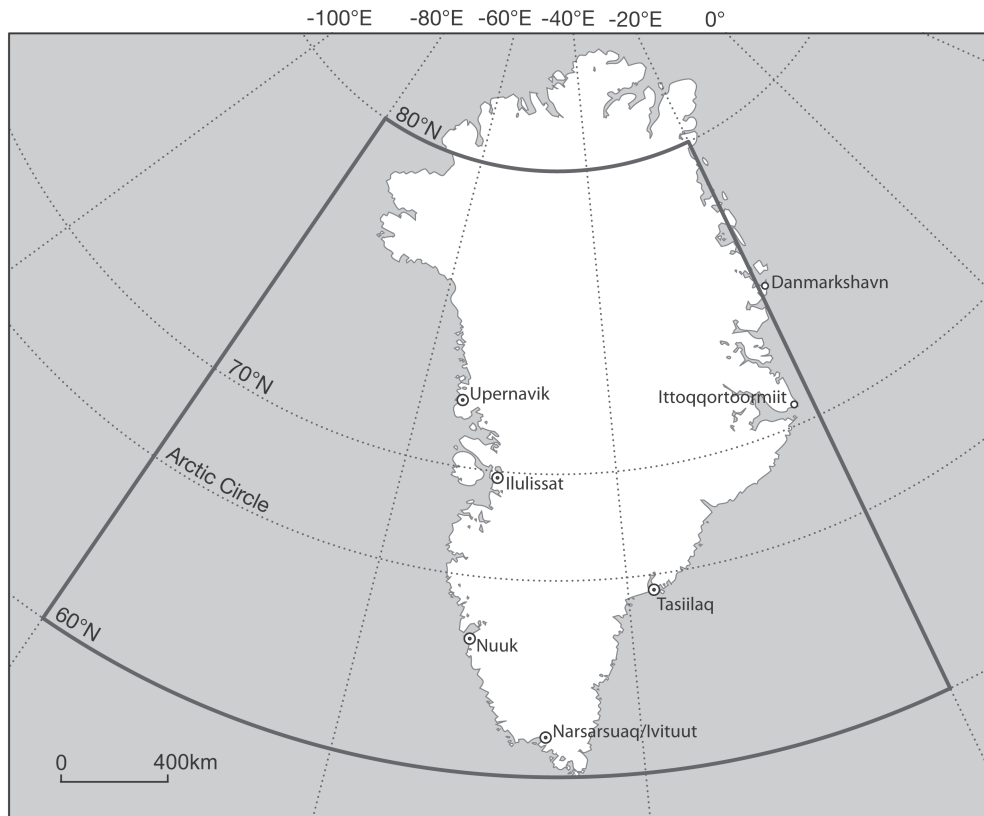
Figure 1. Map showing the Greenland Blocking Index region, and several major Danish Meteorological Institute (DMI) weather stations. Five DMI stations that are used in the calculation of Composite Greenland Temperature 3 (Hanna *et al.*, 2012, 2014) are depicted by a circle surrounding the location points.

2. Methods and datasets

Previously published GBI studies were based on the NCEP/NCAR Reanalysis (which spans from 1948 to near present; Kalnay *et al.*, 2010), so here we used this dataset as our GBI 'baseline' and use 20CRv2c data to extend it backwards in time. This provided a continuous monthly GBI record from January 1851 to December 2015. It was not possible to simply join the 20CR and NCEP–NCAR-based GBI series together as the mean and standard deviation of the two series were not consistent (Table 1). Therefore, for each calendar month, we merged the two GBI time series in a two-stage procedure.

The first step was to homogenize 20CRv2c-based GBI by applying the Bai–Perron structural change point test (Bai and Peron, 2003). This test is able to detect multiple break points, which could arise either through climatic shifts or artificial shifts as an artefact of data assimilation, through changes in the spatial density and number of observations, or through a change in the data-collection method. A breakpoint is determined as non-climatic if it coincides with an estimated inhomogeneity in the time series of the 56-member ensemble standard deviation spread from 20CRv2c, which can act as metadata for the identification of inhomogeneities (Ferguson and Villarini, 2012, 2014). Coincidence of breakpoints was established if there was any overlap of 95% confidence intervals of the breakpoints in GBI and ensemble spread data for

the relevant field. Such breakpoints were corrected for by adding the mean difference between the parts of the time series after and before the breakpoint onto the early part of the series before the breakpoint, and this was done for all necessary breakpoints (there can be more than one breakpoint in a given monthly series). In practice, only 5 months needed correcting: April (1942 breakpoint), May (1942), June (1916), July (1876 and 1917) and August (1874 and 1918). The results were checked using the Pettitt test, Standard Normal homogeneity test and Buishand range test. While these tests only identify a single breakpoint they can also be applied to subsections of the data to identify further breaks. The corrected time series were tested again for homogeneity and found to be homogenous. We also used all available long-term reference mean sea-level pressure (MSLP) time series from Greenland coastal synoptic stations (Cappelen, 2015; Figure 1) to help interpret the GBI homogeneity test results. This is a reasonable procedure because SLP from in/around Greenland can be thought to be partly reflective of the 500 hPa geopotential height (GBI) conditions.

Second, for each monthly GBI time series, we splice 20CRv2c GBI with NCEP/NCAR Reanalysis GBI by multiplying the former with a coefficient so that the variances match for the overlap period; the value of the coefficient was iteratively determined. Next, we subtracted the mean of the 20CRv2c values rescaled in the previous step and added the mean of the NCEP/NCAR GBI values,

Table 1. Monthly GBI statistics from NCEP/NCAR and unspliced 20CRv2c reanalyses (raw GBI = geopotential height in metres), and relationship (correlation) between the two sets of GBI, for the common (1948–2014) period.

Month	NCEP/NCAR mean	NCEP/NCAR st dev	20CRv2c mean	20CRv2c st dev	Correlation coefficient
Jan	5113.3	71.4	5116.5	67.6	0.991
Feb	5121.6	83.3	5123.2	78.4	0.992
Mar	5165.9	77.1	5162.4	73.5	0.986
Apr	5273.5	53.2	5270.5	53.5	0.981
May	5392.3	44.2	5393.3	44.2	0.948
Jun	5471.7	43.5	5480.0	43.2	0.968
Jul	5522.2	29.3	5537.2	27.3	0.923
Aug	5492.7	35.1	5503.0	34.3	0.954
Sep	5392.2	37.6	5399.8	37.6	0.971
Oct	5300.3	52.5	5308.2	49.3	0.991
Nov	5213.0	53.5	5222.5	49.9	0.987
Dec	5145.0	76.6	5152.0	73.7	0.994

Our splicing procedure corrects for differences shown here in the respective means and standard deviations. All correlation coefficients are significant at $p \leq 0.05$.

so that the means of the two respective time series also matched. The raw NCEP/NCAR monthly GBI values are retained for the period since 1948. Regression splicing (e.g. Hanna *et al.*, 2006) does not work well in this context because whilst it rescales the mean it does not result in a matched variance. Note that all correlations between the two unspliced reanalysis series are above 0.92; correlations are weakest for July, while several autumn/winter months have values above 0.99 (Table 1).

Following homogenization and splicing of the combined 20CRv2c and NCEP/NCAR Reanalysis GBI 1851–2015 monthly time series, we calculated seasonal GBI series for the standard 3-month meteorological seasons (MAM = spring, JJA = summer, SON = autumn and DJF = winter, where winter refers to the year of the January); seasonal values are based on means of the GBI monthly anomalies normalized to 1951–2000.

We used standard descriptive statistics and correlation analysis to analyse GBI monthly and seasonal variability and trends over the full period and various sub-periods (some of these being standard climatological normal time periods, as well as longer and more recent sub-periods). Correlation is based on linearly detrended data. We use a 5-year running standard deviation metric to analyse temporal changes in GBI variance. Statistical significance is tested using a *t*-test applied to temporal correlation analysis (after Abramowitz and Stegun, 1965), using the standard significance threshold of $p \leq 0.05$. Standard wavelet analysis was also used as a supporting analysis tool on raw and filtered (7-point binomial) data (Grinsted *et al.*, 2004; Veleda *et al.*, 2012). We also analysed extreme high and low GBI values for each month, to establish whether or not there were any unusual changes in the occurrence of extreme GBI years, with a particular focus on the most recent 15 years of record during the period of strong Arctic Amplification. We used the hypergeometric distribution test to establish the statistical significance of runs of extreme GBI values for particular years and seasons, following a similar procedure by Hanna *et al.* (2015). This was done based on two time periods 2001–2015 and 2007–2015 during the present century and recent period of

strong Arctic Amplification and late summer Arctic sea-ice decline (Cohen *et al.*, 2014; Francis and Vavrus, 2015).

We evaluate the strength and changes of correlation between monthly/seasonal GBI and (1) North Atlantic Oscillation (NAO) indices and (2) an updated Composite Greenland Temperature 3 (monthly and seasonal means of surface air temperatures from five weather stations in coastal western and southern Greenland; Hanna *et al.*, 2012, 2014), and discuss whether these comparisons yield possible insights into (1) the connection of Greenland blocking with wider-scale changes in atmospheric circulation over the North Atlantic, extending down to mid-latitudes, and (2) local-regional scale temperature changes around Greenland. For defining NAO we use a newly developed and extended 1850–2015 Azores–Iceland NAO index (Cropper *et al.*, 2015), both because this encompasses our GBI timespan and also as it uses the traditional/preferred southern station node (Azores) whose pressure record is most strongly anti-correlated with that of Iceland (Jones *et al.*, 2003) and is relatively thermally stable throughout the year; alternative southern stations on mainland Iberia are rather off a south–north Atlantic axis and suffer from seasonal continental heating/cooling effects. We also use the Hurrell principal component (PC)-based NAO index because, although it only extends back to 1899, it is more widely representative of MSLP changes across the North Atlantic (Hanna *et al.*, 2015; Hurrell, 2015). Finally, for the three standard summer months (June-August) we employ the Summer NAO (SNAO) index (Folland *et al.*, 2009; Bladé *et al.*, 2012) which is defined as the first empirical orthogonal function (EOF) of the observed summertime extratropical MSLP over the 40–70°N, 90°W–30°E region, and has been demonstrated to better capture NAO patterns and variations and their effects during summer in Northwest Europe and the UK. SNAO is derived from NCEP/NCAR reanalysis and downloaded from climexp.knmi.nl. The Hurrell PC NAO is similarly based on the PC time series of the leading EOF of monthly MSLP but over the much larger region of 20–80°N, 90°W–40°E (Hurrell, 2015).
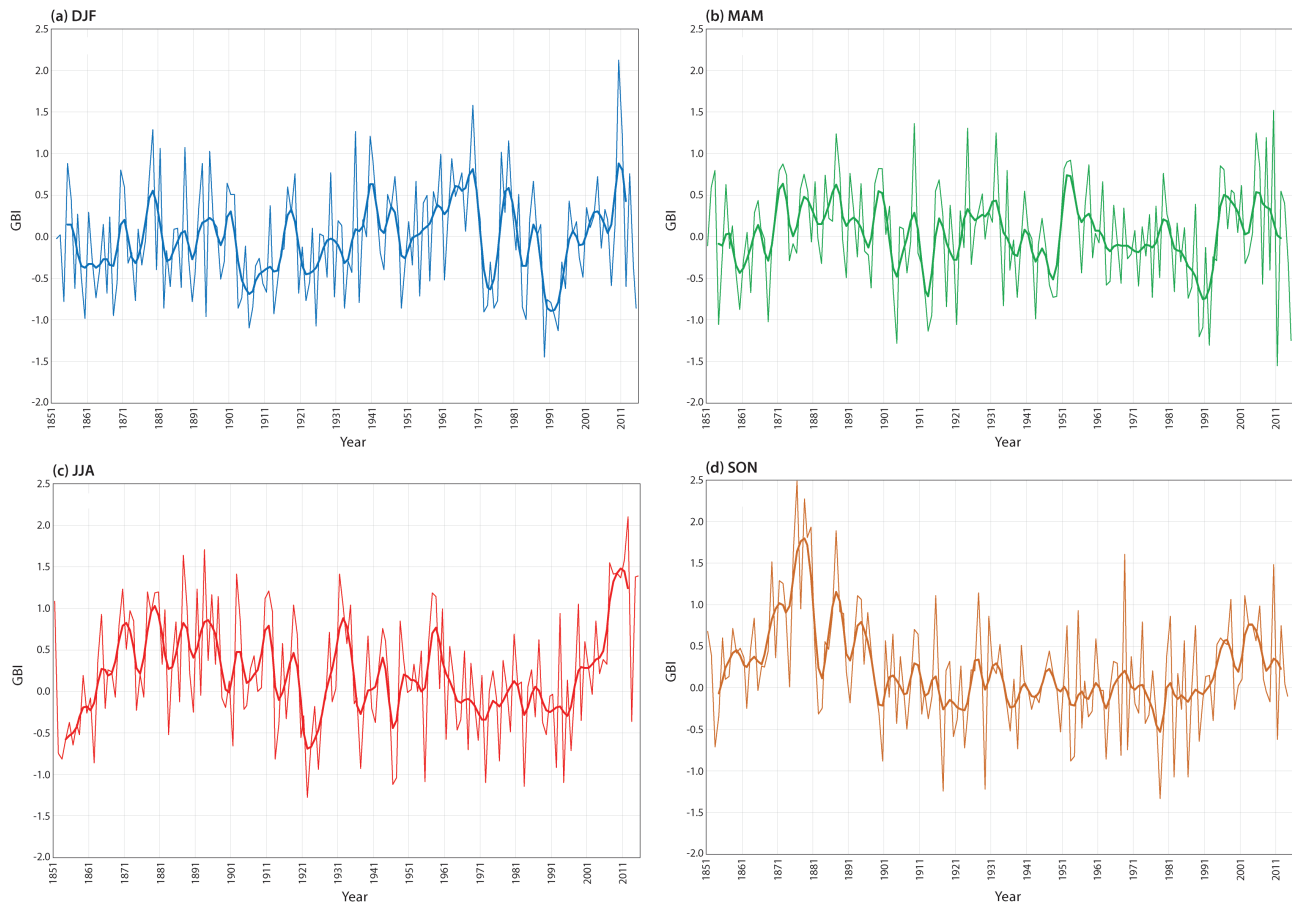
Figure 2. GBI seasonal time series 1851–2015: (a) winter DJF, (b) spring MAM, (c) summer JJA and (d) autumn SON. The overplotted bold lines mark 7-point binomial filters.

The final substantive results section uses composite analysis of high minus low GBI months and seasons to unravel the relationship between physical climate fields at the regional to hemispheric level. A concluding discussion section places our results in a broader-scale contemporary climate-change context.

3. Results

3.1. GBI variability and trends

Figure 2 and Table 2 show seasonal and monthly GBI variability since 1851. Multidecadal peaks and troughs are evident in all four seasonal GBI series (Figure 2). Wavelet plots of GBI series for all 12 calendar months do not show many common sustained features in the raw GBI data (Figure S1). Perhaps the most noteworthy feature is an apparently significant approximately 7- to 8-year period which shows up since about the year 2000 in the December GBI wavelet transform, and also appears in the December NAO wavelet transform (Cropper *et al.*, 2015; Figure S2). However, once the GBI data have been filtered, periods of around 8 years become apparent in most months (Figure 3): although filtering time series naturally emphasizes longer-term periods, this dominant feature is robust to whether a 5-, 7- or 11-point binomial

filter is used (not shown) and also appears in the filtered NAO data wavelets (Figure S3). Cross-wavelet transform plots show a tendency for the NAO to lead GBI, which is especially evident for winter months in the last few decades (Figure S4).

All four seasonal GBI plots show: a peak in the late 19th century around 1880 (although the exact timing of this varies by season), with GBI having risen from a relatively low base in summer and autumn; a trough around 1910 or 1920; another peak or increasing trend around 1930–1940; a generally decreasing – or for autumn rather flat – trend until the 1980s or very early 1990s; and an increase since then (Figure 2). The recent increase is most marked in summer and apparent for winter but displays a mixed signal for autumn and spring – with high values present throughout the first decade of the 20th century but combined with an apparent short-term negative trend during the past decade. Trends in monthly and seasonal GBI for the full period (1851–2015) are all insignificant except for decreases in October, November and autumn (Table 2).

Table 2 also splits the full period into sub-periods for more detailed analysis of monthly and seasonal GBI trends and variability. This shows several significant increases in GBI for 1851–1900 – in May and June and for the year as a whole – whereas there were no significant decreases. For 1901–1950, there are no significant changes. For

Table 2. Monthly and seasonal GBI variability (expressed through standard deviation – sigma) and trends for standard climatological normal and other periods.

Month/Season	Parameter	1851–2015	1851–1900	1901–1950	1951–2000	1981–2010	1991–2015	2001–2015
Jan	Sigma	0.91	0.86	0.89	1.00	0.85	0.75	0.72
	Trend	0.35	0.55	0.83	−0.87	0.76	0.89	0.11
Feb	Sigma	1.03	0.99	1.09	1.00	1.06	1.01	1.07
	Trend	0.19	0.52	0.27	**−1.22**	1.16	1.17	−0.18
Mar	Sigma	0.99	0.88	1.05	1.00	0.98	0.99	1.06
	Trend	−0.30	0.50	0.60	**−1.17**	**1.22**	0.60	−0.66
Apr	Sigma	1.02	0.98	0.97	1.00	1.03	1.22	1.25
	Trend	−0.02	0.10	−0.54	0.22	1.12	−0.77	−0.72
May	Sigma	0.89	0.67	0.87	1.00	1.04	1.14	1.19
	Trend	−0.07	**0.76**	−0.11	−0.39	1.00	−0.03	−0.85
Jun	Sigma	0.98	0.97	0.90	1.00	0.99	1.09	0.94
	Trend	0.38	**1.65**	−0.11	0.06	0.61	1.39	0.95
Jul	Sigma	1.13	1.05	1.26	1.00	1.00	1.14	1.13
	Trend	−0.03	0.68	−0.28	−0.14	**1.63**	**1.86**	**1.97**
Aug	Sigma	0.97	1.00	0.80	1.00	1.03	1.08	0.89
	Trend	−0.16	0.50	−0.36	−0.82	**1.98**	**2.36**	0.56
Sep	Sigma	1.01	1.06	1.00	1.00	0.96	0.83	0.85
	Trend	−0.46	0.56	−0.40	0.37	0.23	−0.78	−1.28
Oct	Sigma	1.04	1.09	0.76	1.00	1.01	0.85	0.85
	Trend	**−0.58**	0.90	0.00	0.52	**1.36**	−0.05	−0.84
Nov	Sigma	1.02	1.14	0.95	1.00	1.00	0.99	0.72
	Trend	**−0.59**	−0.90	0.08	−0.09	0.85	0.41	−0.20
Dec	Sigma	0.93	0.82	0.81	1.00	1.19	1.24	1.43
	Trend	0.11	−0.19	0.70	0.02	1.33	0.17	−0.91
Ann	Sigma	0.42	0.43	0.33	1.00	0.53	0.48	0.48
	Trend	−0.10	**0.47**	0.06	−0.29	**1.11**	0.60	−0.17
DJF	Sigma	0.65	0.61	0.61	0.69	0.70	0.73	0.76
	Trend	0.22	0.27	0.56	**−0.80**	**0.90**	0.91	−0.32
MAM	Sigma	0.61	0.54	0.61	0.57	0.72	0.79	0.90
	Trend	−0.13	0.46	−0.01	−0.45	**1.11**	−0.06	−0.74
JJA	Sigma	0.71	0.68	0.69	0.61	0.73	0.87	0.73
	Trend	0.06	0.00	−0.26	−0.30	**1.42**	**1.87**	1.16
SON	Sigma	0.67	0.73	0.50	0.62	0.62	0.52	0.59
	Trend	**−0.55**	0.00	−0.10	0.27	**0.82**	−0.14	−0.77

Units are normalized GBI values, and trends significant at $p \leq 0.05$ are highlighted in bold.

1951–2000, February, March and winter show significant decreases. We also focus on three more recent periods of more contemporary climate change. Over 1981–2010, all seasons, annual, March, July, August and October had significant GBI increases. For 1991–2015, these GBI increases were sustained for summer, July and August (the sustained summer increase over the last 25 years is clearly seen in Figure 2). There were no significant trends for the shorter recent 2001–2015 period except for an increase in July.

Most monthly and all seasonal time GBI series do not show significant overall (1853–2013) trends in variability; the exceptions are May and December, both with significantly increasing variability (Table 3). Figure 4 shows changes in GBI variability for the seasons and December, with a striking upward trend clearly visible for the latter.

3.2. Changing frequency of extreme GBI values

We next analyse low and high GBI values for each month and season (Table 4). 2010 features as the highest December, winter, spring and annual values in the entire GBI series since 1851 (followed by the record low spring and April values in 2011). 2010 also appears in the highest 10 values in January, February, April, May, August and autumn. Some five of the ten highest summer GBI values occurred between 2007 and 2012, with 2015 and 2014 having the 10th- and 11th highest GBI values in the 165-year summer GBI series. Years since 2001 feature in both the lowest ten and the highest ten December GBI values (there are five extreme years since 2001), which is a symptom of the significantly increasing GBI variability in that month as discussed above.

To test the significance of this recent clustering of extreme GBI values, we use the hypergeometric test and focus on the following seasons and months in which more than two of the highest ten and/or lowest ten extreme values for that month or season occurred since 2000: specifically summer (JJA), June and December (Table 4). For summer, where six of the ten (and 7 of the 11) highest years in the entire record occurred since 2007, this is found to be highly significant in both samples (i.e. for both of the above time periods): this is especially so for 2007–2015 ($p = 0.0001$) but also for 2001–2015 ($p = 0.00370$). These
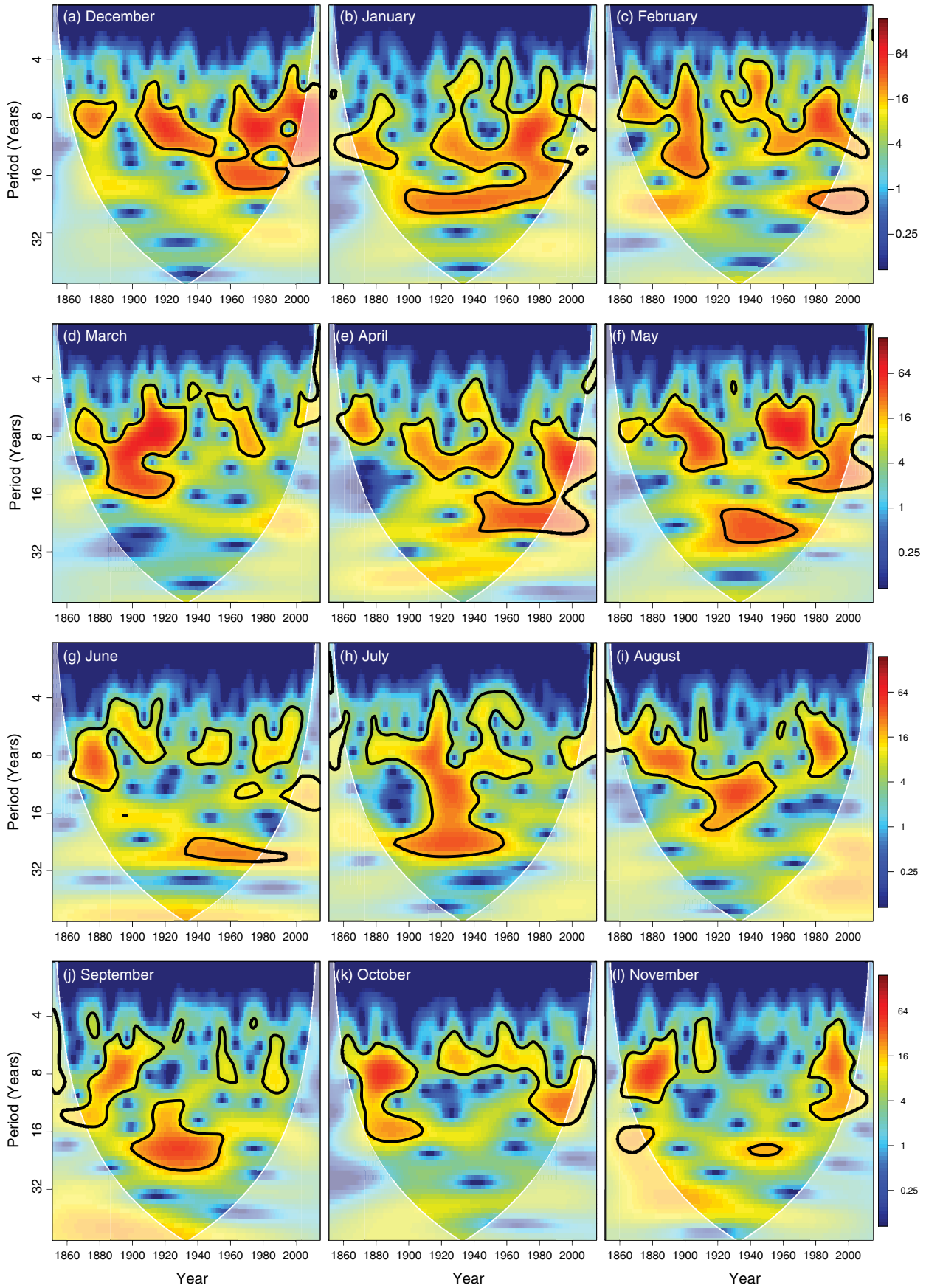
Figure 3. GBI wavelet transforms for all calendar months, based on our new/extended (1851–2015) GBI time series, and a 7-point binomial filter applied to each monthly series.

Table 3. Trends in monthly and seasonal GBI variability (5-year running standard deviation – sigma).

Month/Season	1853–2013	1901–2013	1948–2013	1981–2013	1991–2013	2001–2013
Jan	0.03	0.14	−0.10	−0.55	0.17	0.38
Feb	−0.06	−0.07	−0.15	0.33	0.57	0.49
Mar	0.03	−0.23	−0.04	0.12	0.35	0.34
Apr	0.10	0.23	0.33	0.57	0.85	1.70
May	**0.44**	0.17	0.18	0.60	0.37	0.97
Jun	0.19	0.08	0.34	−0.03	−0.11	0.69
Jul	−0.08	−0.37	−0.44	0.28	−0.17	0.26
Aug	0.12	0.18	−0.14	−0.20	0.38	0.58
Sep	0.14	0.03	−0.17	−0.29	0.14	0.45
Oct	−0.13	0.12	−0.20	−0.10	0.03	−0.19
Nov	−0.18	−0.08	0.04	−0.36	−0.73	0.29
Dec	**0.46**	**0.54**	0.31	0.74	1.23	1.10
Ann	0.03	0.08	0.14	0.06	0.32	0.69
DJF	0.01	0.11	0.10	0.17	0.71	0.94
MAM	0.09	0.02	0.40	0.60	0.68	0.79
JJA	0.06	−0.06	0.00	0.00	−0.16	0.46
SON	0.04	0.06	−0.08	−0.04	0.38	0.40

Units are normalized GBI values, and trends significant at $p \leq 0.05$ are highlighted in bold.
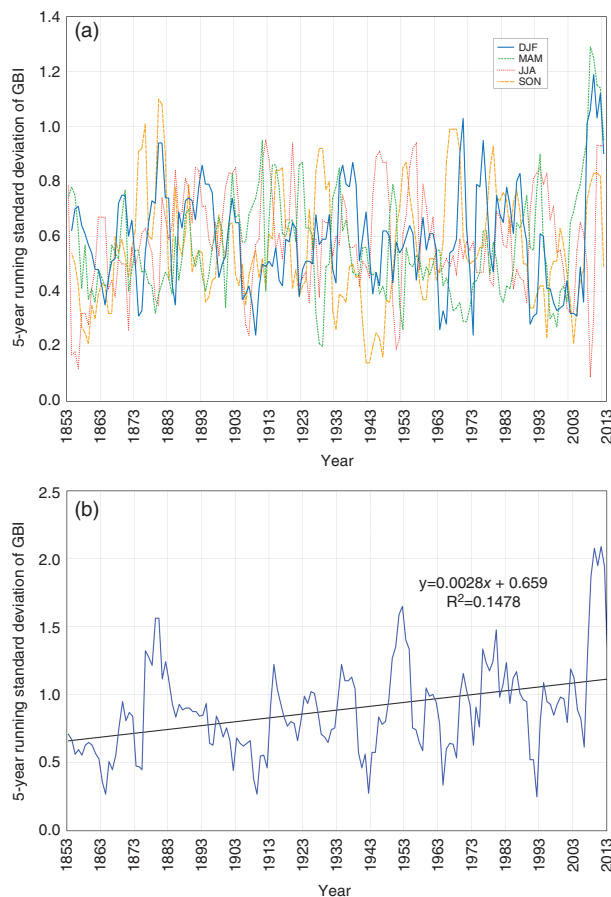

Figure 4. (a) Five-year running standard deviations, 1853–2013, of seasonal GBI; (b) 5-year running standard deviation of December GBI.

significant at the standard $p \leq 0.05$ level. The summer and June GBI series are normally distributed, which engenders high confidence in these results. A similar recent clustering of high summer GBI values is not seen in the August monthly series, and the occurrence since 2007 of three of the ten highest July GBI values is not quite statistically significant; however, all of the recent extreme high summer GBI years also have extreme high June and/or July GBI values, so this does appear to be predominantly an early- to mid-summer phenomenon. Turning our attention to December, we note that 5 (3) of the 20 most extreme (i.e. the ten highest and ten lowest) GBI years occurred since 2001 (2007). The hypergeometric test gives an associated probability of $p = 0.0213$ (0.08), which is significant (just insignificant) for the respective period. The December GBI values are not normally distributed but, because each value in the hypergeometric test is either true or false, the base distribution of the data is not expected to seriously affect the reliability of the results as long as the time series are not strongly autocorrelated (which could enhance clustering of extreme values). The GBI monthly series for June and December are hardly autocorrelated – respective correlation coefficients of the series correlated against themselves displaced by 1 year are 0.18 and −0.12 – and the summer GBI series is similarly only weakly autocorrelated ($r = 0.24$). Therefore, we judge that the GBI has had a significant number of extreme (both high and low) years in December since 2001, and that June and summer have had significant clusterings of high GBI years since 2007 and also since 2001 in the case of summer.

3.3. Relationship between GBI and other climatic indices

Tables 5–7 contain detrended correlation coefficients between GBI and respectively NAO and CGT3 for the same periods as in Table 2. The GBI–NAO correlations are mainly significantly negative. For the station-based

results for summer are supported by a similar analysis for June, for which four of the ten highest GBI values occurred since 2007, with the second highest June GBI in 2012 (Table 4). According to the hypergeometric test the chance probability of getting this clustering of extreme June GBI values during 2007–2015 is 0.0135, which we accept as

NAO (Cropper *et al.*, 2015) for the full (1852–2014) time period, GBI–NAO correlations are strongest in January to March (all below −0.8) and weakest in July at −0.37 (Table 5). For the two most recent time periods since 1991, correlations for December are below −0.9 and as low as −0.96 for 2001–2014. The month with the least strong correlations (although still significant for the overall period) is July. The time variations in correlation coefficients reflect a mix of non-stationary relationships between the GBI and NAO indices, random fluctuations and/or variations related to data quality. Using the Hurrell PC-based NAO index (Hurrell, 2015), correlation coefficients are generally below −0.7 except for July and August in the earliest (1901–1950) period, when they are slightly higher (i.e. less strong; Table 6). Correlations reach an impressive −0.94 for 1951–2000 (February and December), −0.96 for February and December 1981–2010, −0.96 for December 1991–2014, and −0.97 for December 2001–2014. For the full period (1899–2014) of Hurrell PC NAO data availability, GBI–NAO correlations range from −0.75 in July to −0.94 in February and December. Using the SNAO index (Folland *et al.*, 2009; Bladé *et al.*, 2012) slightly improves the GBI–NAO correlations in June from −0.86 (−0.64) to −0.93 compared with using Hurrell PC NAO (Azores–Iceland NAO) index, based on 2001–2014, but this is not the case for July and August values or for longer/earlier time series.

GBI–CCT3 correlations are all positive, nearly all significantly so except for one instance June in the 2001–2014 period (Table 7). There is no clear or consistent seasonal cycle in these correlations but they hold up well for the earlier periods (Table 7). Strong correlations have been found between winter temperatures across southwestern Greenland and high blocking activity in the Greenland/North Atlantic region by Rimbu and Lohmann (2011). The same authors also identified a typical pattern of an out-of-phase relationship between blocking frequency and the NAO – mirroring the strongly negative NAO–GBI relationship that we have found here. However, the authors also note the potential for the occurrence of synoptic conditions where North Atlantic blocking can also be associated with a positive NAO, although the centre of the block would typically be shifted more towards the UK than centred over Greenland.

3.4. GBI composite analysis

Northern Hemisphere plots of various meteorological parameters (geopotential height at 850, 700, 500 and 300 hPa), 850 hPa (near-surface) temperature, precipitation, 500 hPa wind, omega and sensible and latent heat fluxes) are examined for the ten highest minus the ten lowest GBI years for the main seasons, and two months June and December highlighted above as being of special interest. Only the plots for winter and summer are shown in the main text (Figures 5 and 6) but for completeness the other seasons' and June and December plots are presented in Figures S5–S8. The impact of GBI changes on geopotential height (GPH) is clearly greatest in winter (when the circulation is strongest and most variable), and the focus of maximum GPH difference is greatest just off of southeast Greenland, compared with southwest Greenland in the summer difference plots. In terms of broader hemispheric circulation features, high GBI is associated with moderate troughing over central Europe in winter but only weaker troughing displaced north and west to the UK and westwards regions in summer. Also with high winter GBI, low heights are focused in the north-east Pacific off the west Canadian coast.

Temperature anomalies under a high GBI regime are high over Greenland and the Labrador Sea, partly because greater GPH heights are thermodynamically linked to higher temperatures (e.g. Overland *et al.*, 2015, supported by the strong positive correlations in our Table 7) but in winter this anomaly extends further west to encompass Hudson Bay and the surrounding regions. The accompanying negative winter temperature anomaly over Siberia, Scandinavia and the UK is equally striking. However, in summer the temperature high is much more restricted and in Greenland is only really high along the west coast and extending out over the Labrador Sea; there is also a pronounced warm anomaly around the north Russia coast and a cold anomaly over northern Canada, in contrast to winter.

Precipitation anomalies are mainly positive over Greenland under high GBI because milder, moister southerly winds are then advected over the Ice Sheet. This situation reverses for southern Greenland in summer, which has a distinct dry anomaly. This reflects the seasonal northward migration and general weakening of the northern polar jet stream between winter and summer, with negative precipitation anomalies (linked with the jet and a negative NAO) under a positive GBI migrating north towards Greenland. This seasonal change is accompanied by opposite precipitation anomalies over much of the UK (most evident and predominantly wet in summer but tending towards dry in winter) linked with high GBI. Hanna *et al.* (2008) and the UK Met Office (2012) document the exceptionally wet 2007 and 2012 UK summers, and Overland *et al.* (2012) discuss how the recent run of wet UK summers may be linked to recent jet stream anomalies, a high GBI and positive Arctic Dipole. However, it is clear from its geographical position that the UK is very sensitive to slight changes in GBI and associated precipitation anomalies, especially in winter.

The collective winter plots in particular show clear elements of the Scandinavian or Eurasia-1 and East Atlantic circulation patterns, for example with the southern temperature anomaly displaced eastwards to give a distinct southeast-northwest temperature dipole (Barnston and Livezey, 1987).

The 500 hPa wind anomaly plots show an easterly anomaly over much of the mid-North Atlantic that is again related to a weak jet stream under high GBI, and again this is most evident in winter. In summer, the predominant westerly circulation over the UK does not weaken under high GBI and actually an anomalous anticlockwise/cyclonic circulation is then apparent. Sensible

Table 4. Lowest 10 and highest 10 GBI years for each month and season (based on January 1851–December 2015).

Month/Season	Lowest 10	Highest 10
Jan	1993, 1933, 1984, 1989, 1957, 1860, 1983, 1877, 1911, 1928	1929, 1969, 1945, 1959, 1881, **2010**, 1940, 1977, 1888, 1980
Feb	1989, 1935, 1854, 1990, 1894, 1997, 1959, 1868, 1883, 1910	1947, 1901, **2010**, 1902, 1895, 1942, 1960, 1855, 1900, 1965
Mar	1986, 1913, 1920, 1989, 1921, 1907, 1948, 1990, 1857, 1994	1962, 1909, **2013**, 1915, 1916, 1856, 1900, 1958, 1932, 1870
Apr	**2011**, 1897, 1990, 1949, 1904, 1947, 1860, 1943, 1938, 1863	1953, 1995, 1979, 1873, 1920, 1996, 1884, 1924, **2008**, **2010**
May	1956, 1992, 1963, 1914, 1934, **2015**, 1989, 1970, **2009**, 1971	1894, **2010**, **2008**, 1952, 1954, 1928, 1906, 1909, 1932, 1993
Jun	1922, 1994, 1972, 1862, 1978, 1946, 1967, 1914, 1858, 1970	1897, **2012**, 1891, 1998, 1902, **2011**, **2007**, **2008**, 1982, 1903
Jul	1955, 1925, 1964, 1946, 1916, 1926, 1941, 1857, 1852, 1970	1918, **2009**, **2015**, 1880, 1962, 1919, 1893, **2012**, 1869, 1993
Aug	1853, 1976, 1991, 1983, 1937, 1992, 1900, 1913, 1961, 1972	1877, 1966, **2010**, 1887, 1931, 1893, 1885, 1960, **2011**, 1872
Sep	1982, 1853, 1963, 1989, 1974, 1969, 1923, 1900, 1975, 1950	1876, 1930, 1877, 1887, 1894, 1998, 1889, 1872, 1968, 1927
Oct	1986, 1957, 1953, 1929, 1963, 1854, 1904, 1938, 1935, 1978	1880, 1888, 1896, 1879, **2006**, 1878, 1894, 1892, 1869, 1955
Nov	1978, 1993, 1920, 1986, 1913, 1894, 1992, 1853, 1907, 1982	1878, 1876, 1879, 1875, 1869, 1871, 1947, 1901, 1965, 1915
Dec	1953, **2011**, 1936, 1932, 1951, 1972, 1905, 1924, **2004**, 1984	**2010**, 1878, **2009**, 1978, 1961, **2001**, 1952, 1950, 1996, 1916
Ann	1989, 1913, 1854, 1972, 1992, 1904, 1921, 1990, 1986, 1914	**2010**, 1878, 1887, 1879, **2012**, 1872, 1880, 1888, 1870, 1968
DJF	1989, 1993, 1906, 1925, 1984, 1860, 1894, 1992, 1868, 1913	**2010**, 1969, 1879, 1936, 1940, **2011**, 1979, 1888, 1881, 1895
MAM	**2011**, 1992, 1904, **2015**, 1989, 1913, 1990, 1854, 1921, 1868	**2010**, 1909, 1924, **2005**, 1932, 1887, **2008**, 1953, 1952, 1872
JJA	1922, 1983, 1946, 1972, 1994, 1955, 1947, 1925, 1937, 1992	**2012**, 1893, 1887, **2011**, **2007**, **2009**, **2008**, 1931, 1902, **2015**
SON	1978, 1917, 1929, 1982, 1986, 1900, 1953, 1963, 1954, 1967	1876, 1878, 1880, 1887, 1879, 1875, 1968, 1869, **2010**, 1871

Years since 2000 are highlighted in bold.

Table 5. Detrended correlation coefficients between monthly and seasonal GBI and Cropper *et al.* (2015) Azores–Iceland NAO, for standard climatological normal and other periods.

Month/Season	1852–2014	2001–2014	1991–2014	1981–2010	1951–2000	1901–1950	1852–1900
Jan	−0.81	−0.83	−0.68	−0.74	−0.83	−0.87	−0.76
Feb	−0.87	−0.88	−0.83	−0.89	−0.88	−0.88	−0.84
Mar	−0.81	−0.89	−0.83	−0.83	−0.79	−0.83	−0.77
Apr	−0.66	−0.55	−0.58	−0.65	−0.67	−0.73	−0.70
May	−0.69	−0.86	−0.78	−0.67	−0.77	−0.82	−0.48
Jun	−0.69	−0.64	−0.62	−0.64	−0.75	−0.75	−0.62
Jul	−0.37	*−0.36*	−0.41	−0.41	−0.43	−0.47	−0.31
Aug	−0.47	−0.81	−0.63	−0.55	−0.49	−0.41	−0.53
Sep	−0.60	*−0.36*	−0.41	−0.52	−0.62	−0.65	−0.64
Oct	−0.71	−0.81	−0.82	−0.81	−0.78	−0.74	−0.69
Nov	−0.77	−0.65	−0.76	−0.82	−0.81	−0.81	−0.74
Dec	−0.79	−0.96	−0.92	−0.89	−0.77	−0.76	−0.72
Ann	−0.60	−0.86	−0.79	−0.79	−0.75	−0.57	−0.60
DJF	−0.83	−0.96	−0.89	−0.83	−0.83	−0.83	−0.81
MAM	−0.70	−0.83	−0.76	−0.79	−0.70	−0.82	−0.63
JJA	−0.40	−0.72	−0.50	−0.37	−0.42	−0.42	−0.36
SON	−0.60	−0.69	−0.52	−0.63	−0.70	−0.60	−0.61

All coefficients are significant at $p \leq 0.05$ except for those highlighted in italics.

Table 6. Detrended correlation coefficients between monthly GBI and Hurrell PC NAO – and between monthly GBI and monthly Summer NAO (Folland *et al.*, 2009) in brackets for June–August – for standard climatological normal and other periods.

Month	1899–2014	2001–2014	1991–2014	1981–2010	1951–2000	1901–1950
Jan	**−0.92**	**−0.85**	**−0.86**	**−0.90**	**−0.93**	**−0.92**
Feb	**−0.94**	**−0.94**	**−0.92**	**−0.96**	**−0.94**	**−0.93**
Mar	**−0.90**	**−0.98**	**−0.95**	**−0.94**	**−0.89**	**−0.91**
Apr	**−0.85**	**−0.92**	**−0.89**	**−0.85**	**−0.84**	**−0.84**
May	**−0.88**	**−0.94**	**−0.87**	**−0.89**	**−0.91**	**−0.87**
Jun	**−0.87**	−0.86 (**−0.93**)	**−0.89** (−0.83)	**−0.88** (−0.80)	**−0.87** (−0.75)	**−0.85**
Jul	**−0.75**	**−0.84** (−0.79)	**−0.83** (−0.77)	**−0.78** (−0.69)	**−0.81** (−0.43)	**−0.68**
Aug	**−0.76**	**−0.87** (−0.54)	**−0.75** (*−0.24*)	**−0.76** (*−0.29*)	**−0.82** (−0.49)	**−0.59**
Sep	**−0.83**	**−0.71**	**−0.78**	**−0.83**	**−0.87**	**−0.82**
Oct	**−0.87**	**−0.89**	**−0.86**	**−0.87**	**−0.87**	**−0.85**
Nov	**−0.87**	**−0.89**	**−0.87**	**−0.88**	**−0.89**	**−0.86**
Dec	**−0.94**	**−0.97**	**−0.96**	**−0.96**	**−0.94**	**−0.93**

Monthly coefficients that are the highest out of the NAO indices in Tables 5 and 6 are highlighted in bold. All coefficients are significant at $p \leq 0.05$ except for those highlighted in italics.

and latent heat flux (SH and LH) anomalies – which are plotted here as positive upwards from the surface – are negative south of Greenland and positive around the UK and Scandinavia (SH) and southwest of the UK (LH) in winter, with much weaker anomalies in summer. This reflects much lower (higher) sea-air winter heat release around Greenland (UK) under conditions of positive GBI and higher (lower) near-surface temperatures. Finally, omega anomalies are more consistent between winter and summer, being mainly positive in east and extreme southwest Greenland (indicating descending air motion), with negative omega (marking positive vorticity advection and ascending air motion, e.g. Holton, 1992) to be found further north in west Greenland.

To summarize this section, extreme GBI events are clearly linked both thermodynamically and dynamically, with pronounced meteorological anomalies via polar jet-stream changes both downstream and upstream of the Greenland block, and have major repercussions for weather conditions experienced at mid-latitudes. Thus,

the GBI temporal changes noted here have a much wider Northern Hemisphere climatological significance well beyond the Greenland region.

4. Discussion/Summary

The new homogenized/extended GBI time series here should be of wide interest and use to climatological researchers. Our key results from analysing this new time series are that GBI has significantly increased in summer and become significantly more variable with an unusual run of recent extreme values (since 2001) in December. These are in line with previous findings (Hanna *et al.*, 2014, 2015), which are mainly related to the strongly associated NAO (Tables 5 and 6), but are here based on a much longer, homogenized GBI time series dating back to 1851. In this section, we explore possible reasons for these changes and what this tells us about current climate-change processes. Enhanced Greenland blocking may arise from

(a) GPH850

(f) T850

Geopotential Height anomaly (m)
−150 −90 −30 30 90 150

Temperature anomaly (°C)
−4.0 −2.4 −0.8 0.8 2.4 4.0

(b) GPH700

(g) Precipitation

Geopotential Height anomaly (m)
−150 −90 −30 30 90 150

Precipitation anomaly (mm season^{-1})
−100 −60 −20 20 60 100

(c) GPH500

(h) 500 hPa Wind

Geopotential Height anomaly (m)
−150 −90 −30 30 90 150

Wind speed anomaly (ms^{-1})
0 2 4 6 8

9

(d) GPH300

(i) Omega

Geopotential Height anomaly (m)
−150 −90 −30 30 90 150

Omega anomaly (Pascals^{-1})
−1.8 −1.0 0 1.0 1.8

(e) Sensible Heat

(j) Latent Heat

Sensible Heat Flux anomaly (Wm^{-2})
-28 -20 -12 -4 4 12 20 28

Sensible Heat Flux anomaly (Wm^{-2})
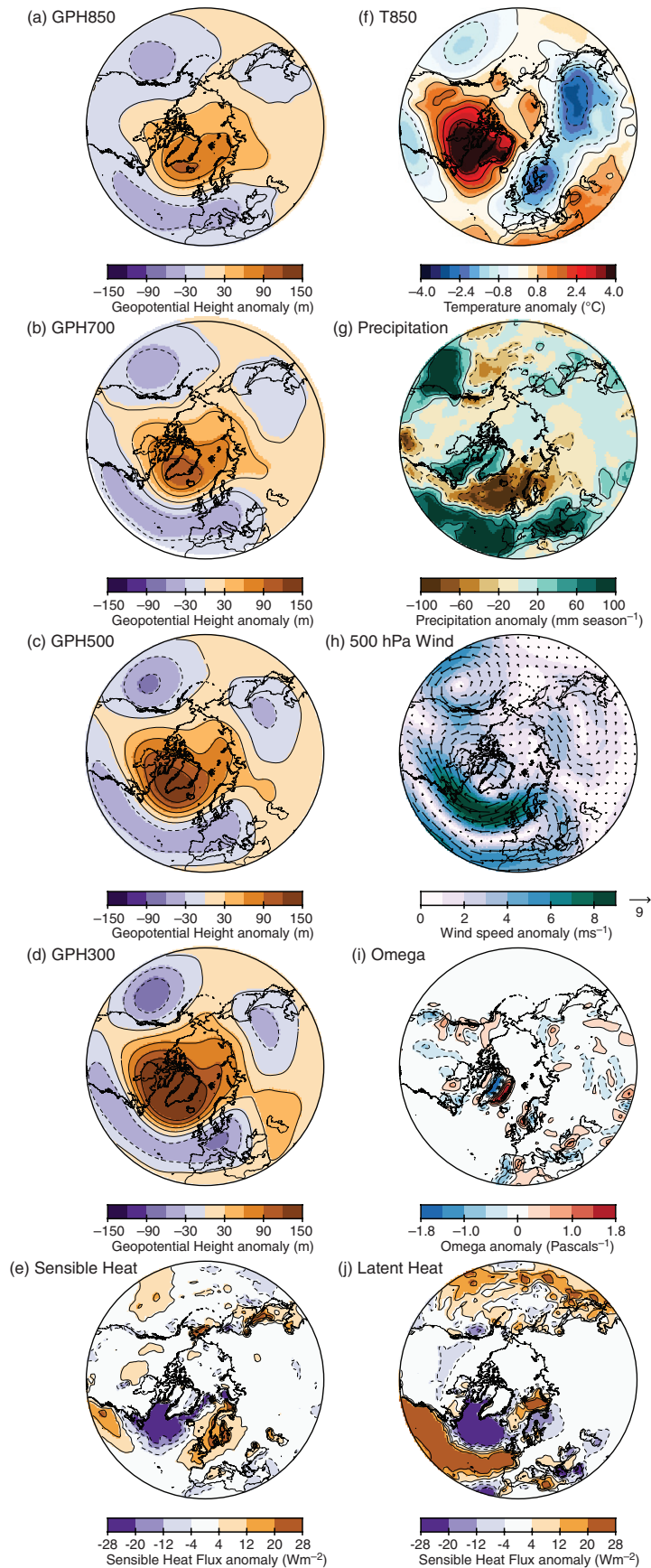-28 -20 -12 -4 4 12 20 28

Figure 5. Difference in various meteorological parameters for the mean of the ten highest GBI years minus the mean of the ten lowest GBI years for winter (DJF).
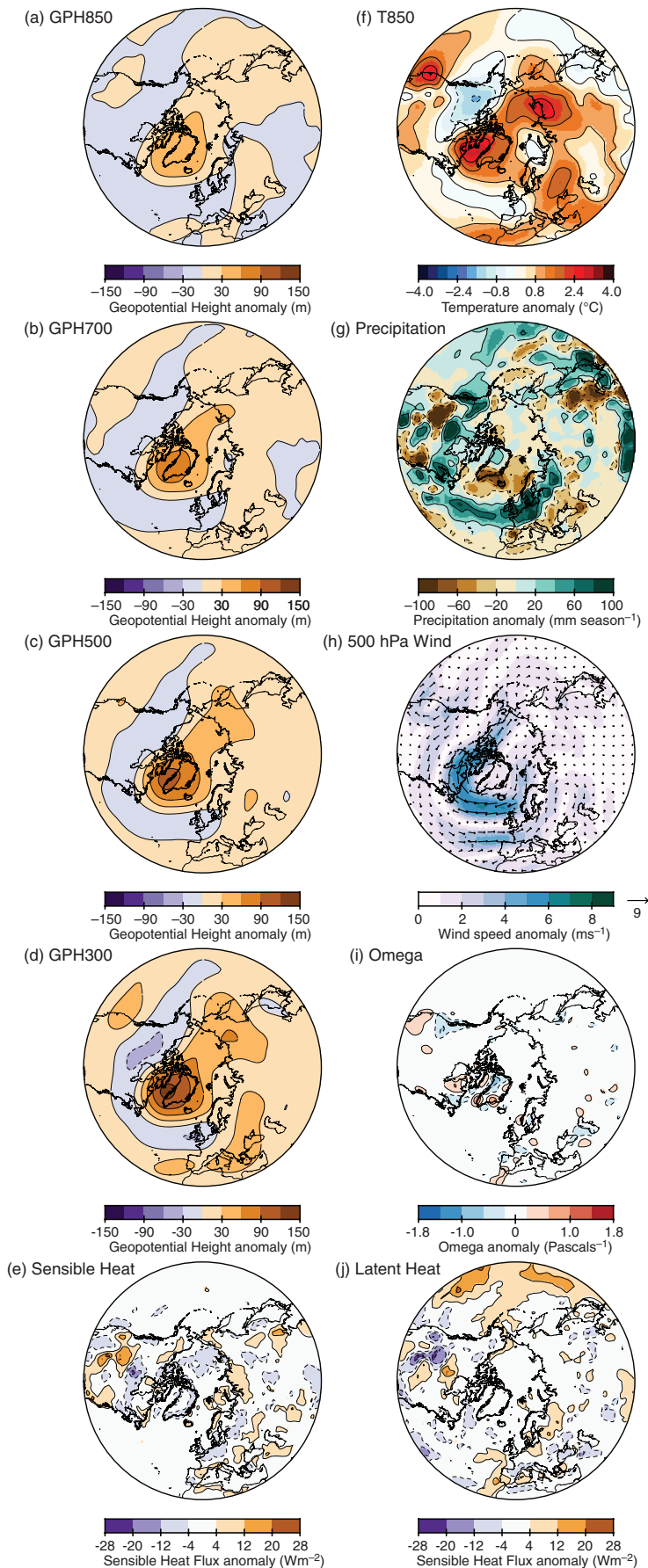
(a) GPH850

(f) T850

−150 −90 −30 30 90 150
Geopotential Height anomaly (m)

−4.0 −2.4 −0.8 0.8 2.4 4.0
Temperature anomaly (°C)

(b) GPH700

(g) Precipitation

−150 −90 −30 **30 90 150**
Geopotential Height anomaly (m)

−100 −60 −20 20 60 100
Precipitation anomaly (mm season^{-1})

(c) GPH500

(h) 500 hPa Wind

−150 −90 −30 30 90 150
Geopotential Height anomaly (m)

0 2 4 6 8 9
Wind speed anomaly (ms^{-1})

(d) GPH300

(i) Omega

-150 -90 -30 30 90 150
Geopotential Height anomaly (m)

-1.8 -1.0 0 1.0 1.8
Omega anomaly (Pascals^{-1})

(e) Sensible Heat

(j) Latent Heat

-28 -20 -12 -4 4 12 20 28
Sensible Heat Flux anomaly (Wm^{-2})

-28 -20 -12 -4 4 12 20 28
Sensible Heat Flux anomaly (Wm^{-2})

Figure 6. Difference in various meteorological parameters for the mean of the ten highest GBI years minus the mean of the ten lowest GBI years for summer (JJA).

Table 7. Detrended correlation coefficients between monthly and seasonal GBI and Composite Greenland Temperature 3 (CGT3; Hanna *et al.*, 2012, 2014), for standard climatological normal and other periods. CGT3 is a mean of the five western and southern Greenland weather stations shown in Figure 1.

Month/Season	1895–2014	2001–2014	1991–2014	1981–2010	1951–2000	1901–1950
Jan	0.64	0.65	0.69	0.79	0.69	0.56
Feb	0.71	0.80	0.77	0.80	0.67	0.71
Mar	0.68	0.67	0.73	0.66	0.65	0.67
Apr	0.63	0.94	0.89	0.75	0.67	0.65
May	0.61	0.70	0.71	0.61	0.74	0.57
Jun	0.63	**0.48**	0.57	0.60	0.65	0.70
Jul	0.55	0.85	0.74	0.72	0.68	0.40
Aug	0.64	0.62	0.58	0.73	0.67	0.58
Sep	0.69	0.82	0.53	0.73	0.74	0.69
Oct	0.66	0.63	0.69	0.70	0.74	0.64
Nov	0.63	0.78	0.78	0.80	0.78	0.47
Dec	0.66	0.94	0.78	0.76	0.76	0.43
Ann	N/A	N/A	N/A	N/A	N/A	N/A
DJF	0.69	0.83	0.78	0.80	0.77	0.57
MAM	0.59	0.86	0.78	0.60	0.55	0.67
JJA	0.60	0.82	0.73	0.76	0.72	0.43
SON	0.63	0.82	0.70	0.68	0.71	0.59

All coefficients are significant at $p \leq 0.05$ except for one value highlighted in bold.

thermodynamic and dynamic influences, although in reality both work together and the balance and interplay of these effects is hard to decipher. However, Rajewicz and Marshall (2014) attribute around 38–49% of Greenland summer air temperature and melt extent variability to circulation anomalies, with lower tropospheric background warming explaining 13–27%. This background warming is easy to explain, as Greenland has been one of the fastest-warming regions of the Northern Hemisphere in the last 10–25 years (e.g. Hanna *et al.*, 2012, 2014; Cohen *et al.*, 2014; Overland *et al.*, 2014). As Greenland warms, warm air expands and raises geopotential heights, which on average increases the intensity and frequency of high pressure: here we see this effect in summer/June, in line with previous observational results (e.g. Francis and Vavrus, 2012; Overland *et al.*, 2012; Hanna *et al.*, 2013, 2014). At the same time, Arctic Amplification of global warming has recently been linked to a sometimes more wavy, meridional and slower-moving jet stream and more negative NAO (e.g. Cohen *et al.*, 2014; Francis and Vavrus, 2015; Overland *et al.*, 2015). This slower-moving jet is associated with stronger blocking features over both Greenland and Siberia, although working out the cause and effect of such jet stream and blocking changes is far from straightforward and requires significant additional dynamical insights (Hall *et al.*, 2015; Overland *et al.*, 2015); moreover, the apparent waviness is contentious and may be metric- dependent (e.g. Barnes, 2013; Screen and Simmonds, 2013).

Multidecadal variations of the GBI are – especially in winter - partly related to similar, 10- to 20-year variations in NAO (not shown), and to longer-period variations in the Atlantic Multidecadal Oscillation (AMO). Hakkinen *et al.* (2011) found that winters with more frequent blocking between Greenland and western Europe are related to a warmer, saltier subpolar North Atlantic ocean and

a positive phase of the AMO – for example during the 1960s, late 1970s and early 2000s – and these are times of high and/or increasing GBI (Figure 2(a)). A 20-year periodicity in blocking frequency over the Scandinavian region has also been linked to solar variability (Rimbu *et al.*, 2014), although our GBI wavelet analysis shows no evidence of a sustained cycle of this length: this is perhaps unsurprising given the difference in regional foci. Although here we only do a formal statistical comparison between GBI and NAO variations, changes in GBI are clearly related to wider North Atlantic blocking and circulation changes, including the East Atlantic and Scandinavian patterns, as revealed through earlier work (Scherrer *et al.*, 2006; Hakkinen *et al.*, 2011; Rimbu *et al.*, 2014).

The greater variability in December GBI and extreme GBI events in recent Decembers is linked to more positive GBI on average, in line with the negative trend in the NAO since 2000 (Hanna *et al.*, 2015) and the more variable December NAO and Arctic Oscillation (AO) over the last few decades (Hanna *et al.*, 2015; Overland and Wang, 2015). The causes of this are at present unclear, and may be related to Arctic sea ice loss, particularly in the Barents-Kara Sea region (e.g. Liptak and Strong, 2014; Overland *et al.*, 2015), or to influences from the tropics (Trenberth *et al.*, 2014) or to decadal fluctuations in the North Pacific and Atlantic and atmospheric internal variability (Perlwitz *et al.*, 2015). Sea-ice loss may lead to a destabilization of early winter jet stream arising from particularly large autumn sea-ice losses and increased ocean–atmosphere heat fluxes (the ice-ocean heat flux feedback) in recent years (Overland *et al.*, 2015). This may have led to a greater likelihood in some years of extreme negative AO and NAO December values and concomitant high GBI values (since the GBI and AO/NAO act mainly in antiphase; Hanna *et al.*, 2015) and more meridional/less zonal jet-stream flow. The tropical

influence is from enhanced tropical convection exciting the poleward propagation of Rossby waves, which may result in more persistent climate anomalies in the extra-tropics (Trenberth *et al.*, 2014). Ding *et al.* (2014) identify tropical forcing as a major contributor to recent observed warming over Greenland, via Rossby-wave propagation, associated with the recent negative trend in the winter NAO, and by implication the positive trend in GBI. A recent study suggests that tropical forcing accounted for the positive NAO trend at the end of the twentieth century, which has recently been overshadowed by the impacts of accelerating sea-ice loss (Feldstein and Lee, 2014). The combination of these possible forcing effects through Arctic Amplification, which is traditionally thought to be greatest in winter due to a lagged response to summer sea-ice losses (Deser *et al.*, 2010; Screen and Simmonds, 2010) and limited ice-/snow-melt during the cold season, may have recently led to more frequent destabilization of the winter jet and polar vortex. However, as this does not happen every year, this may have the effect of making the winter atmospheric circulation in mid-high northern latitudes more variable on an interannual basis. This perhaps reflects interplay between the tropical, Arctic and mid-latitude influences outlined above, together with internal atmospheric variability. Future modelling and dynamical process studies should focus on defining the relative influences of the various climatic forcings and feedbacks discussed above on Greenland Blocking changes. However, whatever the causes of these recent changes, our GBI index effectively captures them and enables them to be placed in a longer-term climatic context.

Statement of data availability

The monthly and seasonal GBI series in this paper are available from http://www.sheffield.ac.uk/geography/staff/hanna_edward/gbi

The 20CRv2c data were accessed in January 2016. We plan to revisit and update our GBI online archive at least annually, if not more frequently.

Acknowledgements

Supporting Information

The following supporting information is available as part of the online article:
Figure S1. GBI wavelet transforms for all calendar months, based on our new/extended (1851–2015) GBI time series and raw (unfiltered) GBI values.

Figure S2. NAO wavelet transforms for all calendar months, based on the Cropper *et al.* (2015) NAO time series and raw (unfiltered) NAOI values.
Figure S3. NAO wavelet transforms for all calendar months, based on the Cropper *et al.* (2015) NAO time series and (7-point binomial-filtered) NAOI values.
Figure S4. Cross-wavelet transforms for all calendar months, between our new/extended (1851–2015) GBI time series and the Cropper *et al.* (2015) NAO series, each of which was filtered with a 7-point binomial filter beforehand. Left-pointing arrows indicate the NAO timeseries leads the GBI and upward (downward) arrows indicate an (in) out of phase relationship.
Figure S5. Difference in various meteorological parameters for the mean of the ten highest GBI years minus the mean of the ten lowest GBI years for spring (MAM).
Figure S6. Difference in various meteorological parameters for the mean of the ten highest GBI years minus the mean of the ten lowest GBI years for autumn (SON).
Figure S7. Difference in various meteorological parameters for the mean of the ten highest GBI years minus the mean of the ten lowest GBI years for the month of June.
Figure S8. Difference in various meteorological parameters for the mean of the ten highest GBI years minus the mean of the ten lowest GBI years for the month of December.

References

Abramowitz M, Stegun IA. 1965. *Handbook of Mathematical Functions: with Formulas, Graphs, and Mathematical Tables*. Dover Books on Mathematics: New York, NY.
Bai J, Peron P. 2003. Computation and analysis of multiple structural change models. *J. Appl. Econ.* **18**: 1–22, doi: 10.1002/jae.659.
Barnes EA. 2013. Revisiting the evidence linking Arctic amplification to extreme weather in midlatitudes. *Geophys Res Lett* **40**: 4734–4739, doi: 10.1002/grl.50880.
Barnston AG, Livezey RE. 1987. Classification, seasonality and persistence of low-frequency atmospheric circulation patterns. *Mon Wea Rev* **115**: 1083–1126, doi: 10.1175/1520-0493(1987)115<1083:CSAPOL>2.0.CO;2.
Bladé I, Liebmann B, Fortuny D, van Oldenborgh GJ. 2012. Observed and simulated impacts of the summer NAO in Europe: implications for projected drying in the Mediterranean region. *Clim. Dyn.* **39**: 709–727, doi: 10.1007/s00382-011-1195-x.
Cappelen J. 2015. Greenland – DMI historical climate data collection 1873–2014 – with Danish abstracts. Technical Report No. 15–04, DMI, Copenhagen, Denmark.
Cohen J, Screen JA, Furtado JC, Barlow M, Whittleston D, Coumou D, Francis J, Dethloff K, Entekhabi D, Overland J, Jones J. 2014. Recent Arctic amplification and extreme mid-latitude weather. *Nat. Geosci.* **7**: 627–637.
Compo GP, Whitaker JS, Sardeshmukh PD, Matsui N, Allan RJ, Yin X, Gleason BE, Vose RS, Rutledge G, Bessemoulin P, Brönnimann S, Brunet M, Crouthamel RI, Grant AN, Groisman PY, Jones PD, Kruk MC, Kruger AC, Marshall GJ, Maugeri M, Mok HY, Nordli Ø, Ross TF, Trigo RM, Wang XL, Woodruff SD, Worley SJ. 2011. The twentieth century reanalysis project. *Q. J. R. Meteorol. Soc.* **137**: 1–28, doi: 10.1002/qj.776.
Compo GP et al. 2015. *NOAA/CIRES Twentieth Century Global Reanalysis Version 2c*. Research Data Archive at the National Center for Atmospheric Research, Computational and Information Systems Laboratory. http://rda.ucar.edu/datasets/ds131.2/ (accessed 8 January 2016).
Cropper L, Hanna E, Valente MA, Jónsson T. 2015. Daily resolution Azores–Iceland station-based North Atlantic Oscillation Index. *Geosci. Data J.* **2**: 12–24.

Davini P, Cagnazzo C, Gualdi S, Navarra A. 2012. Bidimensional diagnostics, variability, and trends of northern hemisphere blocking. *J. Clim.* **25**: 6496–6509, doi: 10.1175/JCLI-D-12-00032.1.

Davini P, Cagnazzo C, Fogli PG, Manzini E, Gualdi S, Navarra A. 2013. European blocking and Atlantic jet stream variability in the NCEP/NCAR reanalysis and the CMCC-CMS climate model. *Clim. Dyn.* **43**: 71–85, doi: 10.1007/s00382-013-1873-y.

Deser C, Tomas R, Alexander M, Lawrence D. 2010. The seasonal atmospheric response to projected Arctic sea ice loss in the late twenty-first century. *J. Clim.* **23**: 333–351, doi: 10.1175/2009JCLI3053.1.

Ding Q, Wallace JM, Battisti DS, Steig EJ, Gallant AJE, Kim H-J, Geng L. 2014. Tropical forcing of the recent rapid Arctic warming in northeastern Canada and Greenland. *Nature* **509**: 209–213, doi: 10.1038/nature13260.

Fang Z-F. 2004. Statistical relationship between the northern hemisphere sea ice and atmospheric circulation during winter time. In *Observation, Theory and Modeling of Atmospheric Variability*. World Scientific Series on Meteorology of East Asia, Zhu X (ed). World Scientific Publishing Company: Singapore, 131–141.

Feldstein SB, Lee S. 2014. Intraseasonal and interdecadal jet shifts in the Northern Hemisphere: the role of warm pool tropical convection and sea ice. *J. Clim.* **27**: 6497–6518, doi: 10.1175/JCLI-D-1400057.1.

Ferguson CR, Villarini G. 2012. Detecting inhomogeneities in the twentieth century reanalysis over the central United States. *J. Geophys. Res.* **117**: D05123, doi: 10.1029/2011JD016988.

Ferguson CR, Villarini G. 2014. An evaluation of the statistical homogeneity of the twentieth century reanalysis. *Clim. Dyn.* **42**: 2841–2866, doi: 10.1007/s00382-013-1996-1.

Folland CK, Knight J, Linderholm HW, Fereday D, Ineson S, Hurrell J. 2009. The Summer North Atlantic Oscillation: past, present and future. *J. Clim.* **22**: 1082–1103.

Francis JA, Vavrus SJ. 2012. Evidence linking Arctic amplification to extreme weather in mid-latitudes. *Geophys. Res. Lett.* **39**: LO6801, doi: 10.1029/2012GL051000.

Francis JA, Vavrus SJ. 2015. Evidence for a wavier jet stream in response to rapid Arctic warming. *Environ. Res. Lett.* **10**: 014005.

Grinsted A, Moore JC, Jevrejeva S. 2004. Application of the cross wavelet transform and wavelet coherence to geophysical time series. *Nonlinear Process. Geophys.* **11**: 561–566.

Hall R, Erdélyi R, Hanna E, Jones JM, Scaife AA. 2015. Drivers of North Atlantic polar front jet stream variability. *Int. J. Climatol.* **35**: 1697–1720, doi: 10.1002/joc.4121.

Hanna E, Jónsson T, Ólafsson J, Valdimarsson H. 2006. Icelandic coastal sea-surface temperature records constructed: putting the pulse on air-sea-climate interactions in the northern North Atlantic. Part 1: comparison with HadISST1 open ocean surface temperatures and preliminary analysis of long-term patterns and anomalies of SSTs around Iceland. *J. Clim.* **19**: 5652–5666, doi: 10.1175/JCLI3933.1.

Hanna E, Mayes J, Beswick M, Prior J, Wood L. 2008. An analysis of the extreme rainfall in Yorkshire, June 2007, and its rarity. *Weather* **63**: 253–260, doi: 10.1002/wea.319.

Hanna E, Mernild SH, Cappelen J, Steffen K. 2012. Recent warming in Greenland in a long-term instrumental (1881–2012) climatic context. I: evaluation of surface air temperature records. *Environ. Res. Lett.* **7**: 045404, doi: 10.1088/1748-9326/7/4/045404.

Hanna E, Jones JM, Cappelen J, Mernild SH, Wood L, Steffen K, Huybrechts P. 2013. The influence of North Atlantic atmospheric and oceanic forcing effects on 1900–2010 Greenland summer climate and ice melt/runoff. *Int. J. Climatol.* **33**: 862–880, doi: 10.1002/joc.3475.

Hanna E, Fettweis X, Mernild SH, Cappelen J, Ribergaard MH, Shuman CA, Steffen K, Wood L, Mote TL. 2014. Atmospheric and oceanic climate forcing of the exceptional Greenland ice sheet surface melt in summer 2012. *Int. J. Climatol.* **34**: 1022–1037, doi: 10.1002/joc.3743.

Hanna E, Cropper TE, Jones PD, Scaife AA, Allan R. 2015. Recent seasonal asymmetric changes in the NAO (a marked summer decline and increased winter variability) and associated changes in the AO and Greenland Blocking Index. *Int. J. Climatol.* **35**: 2540–2554, doi: 10.1002/joc.4157.

Holton JR. 1992. *An Introduction to Dynamic Meteorology*. Academic Press: San Diego, CA, 166–175.

Hurrell JW. 2015. *Hurrell North Atlantic Oscillation (NAO) Index (PC-Based)*. Boulder, CO: National Center for Atmospheric Research. https://climatedataguide.ucar.edu/climate-data/hurrell-north-atlantic-oscillation-nao-index-pc-based (accessed 3 October 2015).

Hakkinen S, Rhines PB, Worthen DL. 2011. Atmospheric blocking and Atlantic multidecadal ocean variability. *Science* **334**: 655–659.

Jones PD, Osborn TJ, Briffa KR. 2003. Pressure-based measures of the North Atlantic Oscillation (NAO): a comparison and an assessment of changes in the strength of the NAO and its influence on surface climate parameters. In *The North Atlantic Oscillation Climatic Significance and Environmental Impact*. American Geophysical Union Geophysical Monograph 134, Hurrell JW, Kushnir Y, Ottersen G, Visbeck M (eds). AGU: Washington, DC.

Kalnay E, Kanamitsu M, Kistler R, Collins W, Deaven D, Gandin L, Iredell M, Saha S, White G, Woollen J, Zhu Y, Leetmaa A, Reynolds R, Chelliah M, Ebisuzaki W, Higgins W, Janowiak J, Mo KC, Ropelewski C, Wang J, Jenne R, Joseph D. 2010. The NCEP/NCAR 40-Year reanalysis project. *Bull. Am. Meteor. Soc.* **77**: 437–471, doi: 10.1175/1520-0477(1996)077<0437:TNYRP>2.0.CO;2.

Liptak J, Strong C. 2014. The winter atmospheric response to sea ice anomalies in the Barents Sea. *J. Clim.* **27**: 914–924, doi: 10.1175/JCLI-D-13-00186.1.

Met Office. 2012. Met Office Confirms Wettest June in Over a Century, *News Release*. Met Office, Exeter, UK. http://www.metoffice.gov.uk/news/releases/archive/2012/wettest-June (accessed April 5 2016).

Overland JE, Wang M. 2015. Increased variability in the early winter subarctic North American atmospheric circulation. *J. Clim.* **28**: 7297–7305, doi: 10.1175/JCLI-D-15-0395.1.

Overland JE, Francis J, Hanna E, Wang M. 2012. The recent shift in early summer arctic atmospheric circulation. *Geophys. Res. Lett.* **39**: L19804, doi: 10.1029/2012GL053268.

Overland J, Hanna E, Hanssen-Bauer I, Kim S-J, Walsh J, Wang M, Bhatt US. 2014. *Air Temperature [In Arctic Report Card 2014]*. www.arctic.noaa.gov/reportcard (accessed April 5 2016).

Overland JE, Francis JA, Hall R, Hanna E, Kim S-J, Vihma T. 2015. The melting Arctic and mid-latitude weather patterns: are they connected? *J. Clim.* **28**: 7917–7932, doi: 10.1175/JCLI-D-14-00822.1.

Perlwitz J, Hoerling M, Dole R. 2015. Arctic tropospheric warming causes and linkages to lower latitudes. *J. Clim.* **28**: 2154–2167, doi: 10.1175/JCLI-D-14-00095.1.

Rajewicz J, Marshall SJ. 2014. Variability and trends in anticyclonic circulation over the Greenland ice sheet, 1948–2013. *Geophys. Res. Lett.* **41**: 2842–2850, doi: 10.1002/2014GL059255.

Rimbu N, Lohmann G. 2011. Winter and summer blocking variability in the North Atlantic region – evidence from long-term observational and proxy data from southwestern Greenland. *Clim. Past* **7**: 545–555.

Rimbu N, Lohmann G, Ionita M. 2014. Interannual to multidecadal Euro-Atlantic blocking variability during winter and its relationship with extreme low temperatures in Europe. *J. Geophys. Res.* **119**: 13621–13636, doi: 10.1002/2014JD021983.

Scherrer SC, Croci-Maspoli M, Schwierz C, Appenzeller C. 2006. Two-dimensional indices of atmospheric blocking and their statistical relationship with winter climate patterns in the Euro-Atlantic region. *Int. J. Climatol.* **26**: 233–249.

Screen JA, Simmonds I. 2010. The central role of diminishing sea ice in recent Arctic temperature amplification. *Nature* **464**: 1334–1337, doi: 10.1038/nature09051.

Screen JA, Simmonds I. 2013. Caution needed when linking weather extremes to amplified planetary waves. *Proc. Natl. Acad. Sci. U.S.A.* **110**: E2327, doi: 10.1073/pnas.1304867110.

Trenberth KE, Fasullo JT, Branstator G, Phillips AS. 2014. Seasonal aspects of the recent pause in surface warming. *Nat. Clim. Change* **4**: 911–916, doi: 10.1038/NCLIMATE2341.

Veleda D, Montagne R, Araujo M. 2012. Cross-wavelet bias corrected by normalizing scales. *J. Atmos. Ocean. Technol.* **29**: 1401–1408.

Wang XL, Feng Y, Compo GP, Swail VR, Zwiers FW, Allan RJ, Sardesmukh PD. 2013. Trends and low frequency variability of extra-tropical cyclone activity in the ensemble of twentieth century reanalysis. *Clim. Dyn.* **40**: 2775–2800, doi: 10.1007/s00382-12-1450-9.